

Solvothermal Magnetic Graphene Oxide for Efficient and Fast Remediation of *p*-Nitroaniline from Industrial Wastewaters

AMR A. YAKOUT^{1,2,*}, DEIA ABD EL-HADY^{1,3}, HASSAN M. ALBISHRI⁴, MEDHAT A. SHAKER^{1,5}, AHMED H. ABDEL-SALAM^{1,2}, ABDELAZIZ S. EL-AHL^{1,6} and MOHAMED E. SABER ALI¹

¹Chemistry Department, Faculty of Science, University of Jeddah, Jeddah, Saudi Arabia

²Chemistry Department, Faculty of Science, Alexandria University, Alexandria, Egypt

³Chemistry Department, Faculty of Science, Assiut University, Assiut, Egypt

⁴Chemistry Department, Faculty of Science, King Abdulaziz University, Jeddah, Saudi Arabia

⁵Chemistry Department, Faculty of Science, Damanhour University, Damanhour, Egypt

⁶Chemistry Department, Faculty of Science, Mansoura University, Mansoura, Egypt

*Corresponding author: Tel: +966 565484044; E-mail: aayhussain@uj.edu.sa; Amryakout157@gmail.com

Received: 11 July 2016;

Accepted: 23 September 2016;

Published online: 29 October 2016;

AJC-18122

Pollution by aromatic compounds such as *p*-nitroaniline in ecosystem has raised significant concerns. A fast and effective removal of *p*-nitroaniline can be carried out by magnetic graphene oxide as a potential sorbent. Different mechanisms including π - π interaction, ion-ion and cation- π bonding interactions have been proposed to describe the strong deposition of *p*-nitroaniline onto magnetic graphene oxide surface. The % removal of *p*-nitroaniline was found to be pH-dependent and attained a maximum value at pH 7.2. The adsorption was best described by Langmuir model with a theoretically estimated maximum adsorption capacity of 482.7 mg g⁻¹, which was very close to the measured value. The adsorption kinetics followed the pseudo-second-order equations very well. The applicability of magnetic graphene oxide for the adsorption of *p*-nitroaniline from industrial wastewater samples was successfully accomplished.

Keywords: Magnetic solid phase extraction, Graphene oxide, Nanosorbent, *p*-Nitroaniline, Industrial wastewaters.

INTRODUCTION

The acute toxicity in aquatic life by aromatic compounds pollutants have been a challenging environmental issue. The existence of even low concentrations of these toxic compounds in water causes an extreme harm to creatures and thus the efficient removal of these poisonous pollutants has become a big environmental problem. Different procedures [1-4] can be followed to remove such pollutants from wastewaters but most of these techniques have many disadvantages such as low efficiency, high cost, long retention times and generation of secondary pollutants. Adsorption technique is proven to be effective method for remediating organic pollutants for its low cost, ease of application and reusability [5-8]. Searching for novel types of adsorbents with fast and efficient capacities toward organic pollutants is one of the main concerns of research scientists. *p*-Nitroaniline is highly toxic with a threshold limit value (TLV) of 0.001 kg/m³ can be found in industrial wastewater discharges either its manufacture or its usage as an intermediate in the production of azo dyes, fuel additives, pesticides, antioxidants, medicines for poultry and antiseptic agents [9,10].

p-Nitroaniline is enlisted as one of the major contaminants in water worldwide and its existence in aquatic environments may cause long-term adverse effects to ecosystem in terms of its splenotoxicity, nephrotoxicity and hematotoxicity [11-13]. Various attempts have been applied to remove *p*-nitroaniline from aqueous media including Fenton oxidation, photocatalytic degradation, biodegradation, hydrothermal decomposition, adsorption and others [14-25]. Graphene (G) and graphene oxide (GO) are nano-scale materials with two-dimensional layers and one-atom thickness. Recently, the wide applicability and wonderful characteristics *e.g.* high mechanical and thermal stabilities, extraordinary electrical and optical properties and high specific surface area of these nanocarbon materials have attracted the attention of many researchers [26-30]. These systems are rich in delocalized π -electron characters that permit strong adsorption for different organic pollutants [31-33]. The vast amount of oxygen-contained groups such as carboxyls, hydroxyls and epoxies on the surfaces of graphene oxide sheets or laterals can increase the interactions between graphene oxide and organic pollutants. Practically, the tiny size of graphene oxide nanosorbents complicates its separation from matrices.

Magnetic solid phase extraction (MSPE) based on nanosorbents can overcome this problem especially in environmental samples in addition to its other advantages such as simple and fast analyte separation with high efficiency for the elimination of toxic pollutants [34-38]. This work reports the use of magnetic graphene oxide to remove of *p*-nitroaniline from an aqueous medium. The effects of different environmental conditions, medium pH, nanosorbent mass and contact time on the removal process were investigated. The reusability and regeneration of magnetic graphene oxide nanosorbent was examined. A complete description of the adsorption process and its mechanism is known from the applications of various isotherm and kinetic models. Also, the applicability of magnetic graphene oxide for adsorbing *p*-nitroaniline from environmental wastewater samples was investigated.

EXPERIMENTAL

Natural graphite (Gt) powder (99.9 %, 500 mesh), FeCl₃·6H₂O, ammonia (22-28 %), *p*-nitroaniline and other materials were purchased from Sinopharm Chemical Reagent Co., Ltd. (China). All chemicals were of analytical grade and used as received. Ultrapure water from a Milli-Q system (Millipore, Billerica, MA) was employed throughout the experiments.

Preparation of magnetic graphene oxide nanoparticles:

Graphene oxide was synthesized using a modified Hummers method [39,40] and exfoliated to afford an aqueous dispersion of graphene oxide under ultrasonication. Briefly, graphite powder was oxidized using KMnO₄/H₂SO₄ and the graphite oxide (GtO) was transformed into graphene oxide by ultrasonication in water. In a typical synthesis process, natural graphite powder (5 g) were mixed with 2.5 g NaNO₃ and 250 mL H₂SO₄ and stirred in a beaker on an ice bath. 15 g of KMnO₄ was added into the mixture slowly and stirred vigorously. The reaction temperature was maintained below 20 °C and the contents were stirred at room temperature over-night. Thereafter, another 15 g of KMnO₄ was added into the mixture and stirred at room temperature to oxidize any unoxidized graphite. Deionized water (250 mL) was slowly added and the temperature was increased to 98 °C and the mixture was maintained at this temperature for 3 h. The reaction was terminated by the addition of 50 mL of 30 % H₂O₂ which turn the solution into yellow colour. The mixture was consequently washed with 100 mL of 5 % HCl and 30 % H₂O₂ five times to remove MnO₂ and sulfates. The product was washed repeatedly with distilled water until pH 7 was achieved. The colour change of the mixture into brilliant yellow indicates the complete oxidation of pristine graphite to the oxide. Finally, the solid was isolated after drying at 60 °C under vacuum. The synthesized oxide was re-dispersed in water to create a yellow-brown dispersion and the transformation of graphite oxide to generate graphene oxide sheets was achieved by ultrasonication for 60 min. The resulting aqueous dispersion of the brown graphene oxide sheet was stable. Magnetic graphene oxide were prepared by hydrothermal method with FeCl₃·6H₂O as a single Fe ion source. 1 g FeCl₃·6H₂O was dissolved in 60 mL ethylene glycol to form a clear solution and then 3.60 g urea and 0.80 g graphene oxide were added to the solution at 50 °C under vigorous stirring for 30 min. The mixture was put into a Teflon-lined

stainless-steel autoclave (60 mL), thereafter the autoclave was heated at 200 °C for 6 h in a furnace and allowed to cool to room temperature. After completion of the reaction, the reaction product was collected with magnet and washed repeatedly with absolute ethanol and deionized water. Finally, the magnetic nanoparticles (MNPs) were dried in vacuum oven at 60 °C for 24 h.

Adsorption experiments: Batch mode experiments were conducted to investigate the effects of medium pH, time and temperature on the adsorption of *p*-nitroaniline onto the magnetic graphene oxide nanoparticles at pre-adjusted conditions using 25 mg aliquots of magnetic graphene oxide added to 25 mL of *p*-nitroaniline (20 mg L⁻¹) and these solutions were agitated with a shaking rate of 250 rpm for a certain period of time. For all determinations, the magnetic nanoparticles were separated from *p*-nitroaniline solution by an external magnet. The residual *p*-nitroaniline concentration in the supernatant was determined by using an UV/visible spectrophotometer at 385 nm. The experiments were done in triplicate and the average was used in calculations. The adsorption capacity of the magnetic graphene oxide (q_e, mg g⁻¹) and percentage *p*-nitroaniline removal efficiency were calculated as follow:

$$\text{PNA removal efficiency (\%)} = \frac{C_i - C_e}{C_i} \times 100 \quad (1)$$

$$q_e = \frac{(C_i - C_e)V}{m} \quad (2)$$

where C_i and C_e (mg L⁻¹) are the initial and equilibrium *p*-nitroaniline concentration, respectively, q_e (mg g⁻¹) is the equilibrium adsorption capacity, V (L) is the *p*-nitroaniline solution volume and m (g) is the mass of the nanosorbent.

RESULTS AND DISCUSSION

Surface morphology and characterization of the magnetic graphene oxide nanoparticles: The representative TEM image of magnetic graphene oxide composite (Fig. 1a) showed that the graphene oxide sheets with a lateral dimension of about 50 nm were decorated with large quantity of Fe₃O₄ nanoparticles. The nanoparticles have irregular mono-dispersed nanoparticles with rough spherical surface to elliptical shape while their size is in the range of 10-20 ± 5 nm. The FTIR spectra of both graphene oxide and magnetic graphene oxide nanosorbents, Fig. 2 showed the O-H stretching vibrational peaks at 3227.3 and 3220.2 cm⁻¹, respectively. For graphene oxide, the peaks at 1170.1 and 1121.4 cm⁻¹ were attributed to C-O stretching vibration of epoxy and alkoxy groups. The peak at 1583 cm⁻¹ was due to the stretching vibration of aromatic C=C; the peaks at 1711.2 and 1400.2 cm⁻¹ were the C=O stretching vibrations of COOH and C=O [41]. These peaks confirm the presence of carboxyl, epoxy groups in graphene oxide. Moreover, the characteristic peak observed at 550.3 cm⁻¹ for magnetic graphene oxide was ascribed to the Fe-O stretching vibration proving that Fe₃O₄ nanoparticles were successfully anchored onto graphene oxide.

The thermal degradation processes of magnetic graphene oxide nanosorbents were studied in the temperature range of 28.4-600 °C by TGA, Fig. 3 identified three different decomposition steps, the first one (28.4-230.5 °C, 4.60 %) is related to the

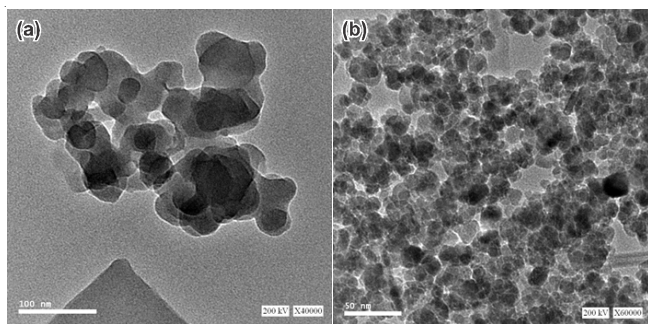


Fig. 1. HRTEM (a) of graphene oxide and magnetic graphene oxide nanoparticles

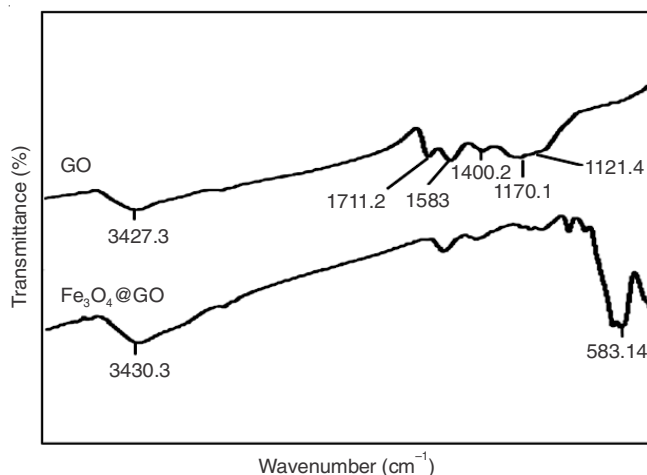


Fig. 2. FTIR of graphene oxide and magnetic graphene oxide nanoparticles

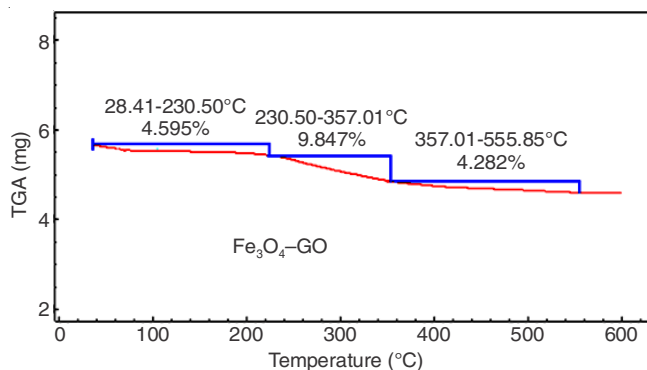


Fig. 3. TGA thermograms of magnetic graphene oxide nanoparticles

desorption of chemically and physically adsorbed H_2O molecules, while the second and third steps (230.5–357.0 °C, 9.85 % and 357.0–555.8 °C, 4.28 %) are attributed to the direct decomposition of loaded graphene oxide moieties.

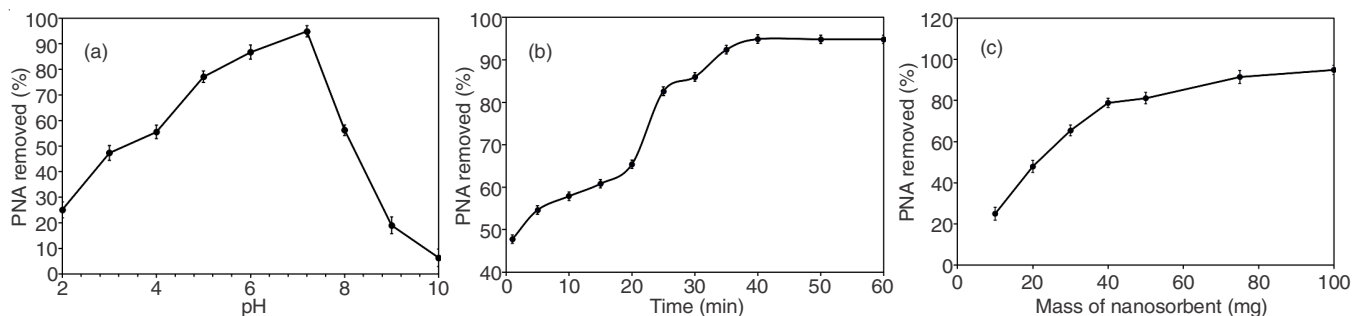


Fig. 4. Effect of pH, contact time and mass of MGO nanoparticles on the percentage PNA removed (25 mL of 20 ppm) at 25 °C

Adsorption batch studies

Effect of pH: The pH effect on the sorption of *p*-nitroaniline onto magnetic graphene oxide surface was tested in the pH range of 2–10 (Fig. 4a). Generally, the percentage of *p*-nitroaniline removal increases gradually with pH and reach to a maximum value at 7.2. The lower values at pH < 4.0 for the removal efficiencies are attributed to the repulsive forces between the functional groups in graphene oxide (-OH, -COOH) and the positive amino groups. The mechanism for strong *p*-nitroaniline adsorption onto magnetic graphene oxide can be explained in terms of π - π , cation- π and ion-ion interactions. The π - π stacking interaction exists between the hexagonal cells of graphene oxide and the ring structure of *p*-nitroaniline [42–45]. The cation- π bonding interaction exists between the π -electron-rich structure of graphene oxide and the protonated amino groups of *p*-nitroaniline [46]. Finally, the ion-ion interaction exists between the negatively charged oxygen functional groups and those protonated amino groups.

Effect of contact time: The effect of contact time on % *p*-nitroaniline removal was investigated by using several time intervals (1, 5, 10, 15, 20, 25, 30, 40, 50 and 60 min) using 100 ± 1 mg dose of magnetic graphene oxide at pH 7.2 (Fig. 4b). It is concluded that the % *p*-nitroaniline removal increases gradually with increasing the contact time. However, *p*-nitroaniline sorption onto magnetic graphene oxide nanoparticles was found to proceed *via* three successive stages and reach a maximum value after 40 min of contact time.

Effect of mass of nanosorbent: The magnetic graphene oxide dose, which plays an important role in the sorption process was also investigated to demonstrate its effect on the percentage removal of *p*-nitroaniline (Fig. 4c). It is obvious that the determined values of the percentage removal of *p*-nitroaniline by magnetic graphene oxide surface increases with increasing the magnetic graphene oxide mass due to the increased availability of active surface functional groups to bind *p*-nitroaniline. A dose of 100 mg magnetic graphene oxide was enough for achieving the highest value (95 %) of the percentage of *p*-nitroaniline removal.

Adsorption isotherms: The experimental results for the *p*-nitroaniline sorption onto magnetic graphene oxide surface were applied to both Langmuir and Freundlich isotherm models for recognizing the suitable model for describing the sorption data and providing information about the effectiveness of PNA-MGO adsorption system. Freundlich adsorption model, expressed as eqn. 7 assumes the existence of different adsorption surface sites with variable interaction energies between the adsorbed species [47]. It is often used for single

solute adsorption systems with heterogeneous energetic distribution of active binding sites in a specific concentration range.

$$q_e = K_F C_e^{1/n} \quad (7)$$

where q_e (mg) is the amount adsorbed of *p*-nitroaniline per 1 g of magnetic graphene oxide adsorbent, C_e is the equilibrium concentration (mg/L), while K_F and n are the model constants. K_F measures the sorption capacity is a function of sorption energy and temperature while n reflects the adsorbent-adsorbate bond strength (adsorption intensity) and can help to determine whether adsorption is favoured. The value $n < 1$ describes unfavourable adsorption, $n > 1$ describes favourable adsorption and $n = 1$ characterizes linear adsorption situations. The linear form of Freundlich isotherm can be expressed by eqn. 8.

$$\log q_e = \frac{1}{n} \log C_e + \log K_F \quad (8)$$

The values of K_F , n and R^2 for the investigated PNA-MGO adsorption system derived from the slope and intercept of the linear plots of eqn. 8 are listed (Table-1). It is concluded that the calculated values of $n > 1$ in addition to the high value of R^2 , Table-1 suggest the favourable adsorption and suitability of Freundlich model to describe the adsorption behaviour in this study. On the other hand, Langmuir model, eqns. 9 and 10 assumes the occurrence of a reversible sorption process in a uniform sorbent surface with limited binding sites to form a monolayer of non-interactive adsorbed species, which occupy separate surface sites with equal affinity and uniform sorption energies [48].

$$q_e = \frac{K_L q_{\max} C_e}{1 + K_L C_e} \quad (9)$$

where C_e (mg L⁻¹) describes the equilibrium concentration of *p*-nitroaniline, q_e (mg g⁻¹) is the *p*-nitroaniline amount adsorbed on magnetic graphene oxide surface at equilibrium, q_{\max} (mg g⁻¹) is the maximum adsorption capacity, which corresponds to a complete monolayer coverage and K_L (L mg⁻¹) is the Langmuir adsorption affinity constant.

$$\frac{C_e}{q_e} = \frac{C_e}{q_{\max}} + \frac{1}{K_L q_{\max}} \quad (10)$$

The values of q_{\max} and K_L , derived from the slope and intercept of the linear plots of C_e/q_e vs. C_e , eqn. 10 are listed in Table-1. The maximum sorption capacity for *p*-nitroaniline was 482.7 mg g⁻¹ (Table-1). The essential characteristics of Langmuir isotherm can be expressed in terms of dimensionless separation factor, F_L using eqn. 11 [49-51].

$$F_L = \frac{1}{1 + K_L C_e} \quad (11)$$

The adsorption nature is unfavourable if $F_L > 1$, linear if $F_L = 1$, favourable if $0 < F_L < 1$ and irreversible if $F_L = 0$. The

calculated F_L values (Table-1) show that for the investigated sorption systems are within the range 0.011-0.004 in the initial *p*-nitroaniline concentration range of 2.0-50 ppm, indicating favourable *p*-nitroaniline sorption onto magnetic graphene oxide. Also, the R^2 values (≈ 1.0) confirm the suitability of Langmuir isotherm model to describe the experimental sorption data and suggest the homogeneous monolayer sorption.

Adsorption kinetics: The experimental kinetic data of *p*-nitroaniline sorption onto magnetic graphene oxide surface were examined using four kinetics models, namely; Lagergren pseudo-first order, pseudo-second order [52,53], Elovich [54] and intra-particle diffusion [55] models. The mathematical equations representing these models are given by eqns. 3-6.

Lagergren pseudo first-order:

$$\ln(q_e - q_t) = \ln q_e - k_1 t \quad (3)$$

Pseudo second-order:

$$\frac{t}{q_t} = \frac{1}{k_2 q_e^2} + \frac{t}{q_e} \quad (4)$$

Elovich:

$$q_t = \frac{1}{\beta} \ln(\alpha\beta) + \frac{1}{\beta} \ln t \quad (5)$$

Intra-particle diffusion:

$$q_t = k_{\text{int}} \sqrt{t} + C \quad (6)$$

where q_e and q_t (mg g⁻¹) are the sorption capacity at equilibrium and time t (min), k is the rate constant and R^2 is the correlation coefficient, expressing the uniformity between the experimental data and the calculated data predicted from the kinetic models, the Elovich constants are the initial adsorption rate, α (mg g⁻¹ min⁻²) and the desorption constant, β (g mg⁻¹ min⁻¹) which is related to the activation energy and the extent of surface coverage for chemisorption and C is the intra-particle diffusion rate constant. All of these kinetic model-derived fitting parameters are collected in Table-2. When comparing the calculated and the experimental values of q_e and the values of correlation coefficients (R^2) of the investigated kinetic models, it can be concluded that the experimental kinetic data follow the pseudo second-order kinetic model very well with higher correlation coefficient ($R = 0.991$). Moreover, it is revealed that the adsorption capacity was proportional to the amount of active sites and the sorption rate-limiting step is controlled by chemical process [56].

Desorption and reusability studies: In practical applications, the desorption extent and regeneration performance of the adsorbent can be determined by both the recycling of the adsorbent and recovery of analyte species. Based on the pH effect, the *p*-nitroaniline sorption onto magnetic graphene oxide surface is insignificant at pH > 10. Therefore, the loaded nanoparticles are re-suspended in NaOH solution (0.1 M)

TABLE-1
DIFFERENT ADSORPTION ISOTHERM PARAMETERS FOR *p*-NITROANILINE (25 mL OF 2-50 ppm)
ONTO MAGNETIC GRAPHENE OXIDE NANOPARTICLES AT 25 °C AND OPTIMUM pH VALUES

Langmuir model				Freundlich model		
q_{\max}	K_L	R_L range	R^2	K_F	n	R^2
482.7	46.38	0.0157-0.0874	0.998	44.08	3.07	0.956

TABLE-2
KINETIC PARAMETERS USED TO ANALYZE THE ADSORPTION OF 20 ppm *p*-NITROANILINE ONTO MAGNETIC GRAPHENE OXIDE NANOPARTICLES

Kinetic models and parameters			
q_e (exp.) (mg g ⁻¹)		4.744	
Pseudo first order		Pseudo second order	
q_e (calc.) (mg g ⁻¹)	5.154	q_e (calc.) (mg g ⁻¹)	4.789
K_1 (min ⁻¹)	1.640	K_2 (min ⁻¹) × 10 ⁻³	12.467
R^2	0.934	R^2	0.991
Elovich		Intra-particle diffusion	
q_e (calc.) (mg g ⁻¹)	3.766	q_e (calc.) (mg g ⁻¹)	3.560
α (mg g ⁻¹ min ⁻²)	1.136	K_{int} (mg g ⁻¹ min ^{-1/2}) ⁻³	0.770
β (g mg ⁻¹ min ⁻¹)	0.867	C	0.118
R^2	0.976	R^2	0.979

with sonication period (5 min) to desorb all *p*-nitroaniline from magnetic graphene oxide nanoparticles. After removing magnetic graphene oxide from NaOH solution using a magnet separation, the *p*-nitroaniline concentration in solution was determined and the percentage recovery of magnetic graphene oxide adsorbent was found to be 99.2 % ± 3.4, indicating a complete desorption of *p*-nitroaniline. To estimate the sorbent reusability, three cycles of adsorption–desorption processes were conducted using the same sorbent and only a loss of 3.6–5.1 % in the removal efficiency was noticed. These results indicate that the magnetic graphene oxide nanoparticles have good reusability and stability.

Extraction of *p*-nitroaniline from real samples: The magnetic solid phase extraction of *p*-nitroaniline from industrial wastewater samples of four different matrices was successfully accomplished by the proposed method and the results of this study are collected in Table-3. The first and second samples are textile dyes wastewaters, the third one is antiseptic wastewater while the fourth sample is agriculture wastewater. The percentages of *p*-nitroaniline removal efficiency for all samples were found to be 94.3–96.6 % ± 2.7–4.2. These results assure the potential application of magnetic graphene oxide nanoparticles for the *p*-nitroaniline removal from various industrial wastewater matrices using batch equilibrium technique.

TABLE-3
MAGNETIC SOLID PHASE EXTRACTION OF *p*-NITROANILINE FROM DIFFERENT INDUSTRIAL WASTEWATER SAMPLES BY 0.100 g OF MAGNETIC GRAPHENE OXIDE NANOPARTICLES

Industrial wastewater sample	Amount detected (µg mL ⁻¹)	(Amount detected after MSPE) % PNA removal efficiency
Sample 1 (Textile dyes wastewater)	2.731	(0.156) 94.29 % ± 3.4
Sample 2 (Textile dyes wastewater)	3.169	(0.107) 96.62 % ± 4.2
Sample 3 (Antiseptic wastewater)	1.077	(0.042) 96.10 % ± 2.7
Sample 4 (Agriculture wastewater)	2.283	(0.114) 95.01 % ± 4.6

Conclusion

This work reports the usage of magnetic graphene oxide nanoparticles for effective *p*-nitroaniline extraction from aqueous media. The magnetic graphene oxide nanoparticles

have good stability, dispersibility and magnetic property. The adsorption processes were fully optimized and found to be affected by pH change significantly. The optimum solution pH for the adsorption of *p*-nitroaniline onto the MNPs was 7.2. The sorption equilibrium was attained within 40 min and well-fitted to Langmuir model. Also, the adsorption kinetics follows the pseudo second order equations. The examined magnetic nanoparticles showed excellent efficiency for *p*-nitroaniline extraction from industrial wastewater samples.

REFERENCES

- M.A. Salam, *J. Ind. Eng. Chem.*, **28**, 67 (2015).
- H.V. Phan, F.I. Hai, J. Kang, H.K. Dam, R. Zhang, W.E. Price, A. Broeckmann and L.D. Nghiem, *Bioresour. Technol.*, **165**, 96 (2014).
- Z. Karim, A.P. Mathew, M. Grahm, J. Mouzon and K. Oksman, *Carbohydr. Polym.*, **112**, 668 (2014).
- H.-T. Fan, Q. Tang, Y. Sun, Z.-G. Zhang and W.-X. Li, *Chem. Eng. J.*, **258**, 146 (2014).
- D. Hank, Z. Azi, S. Ait Hocine, O. Chaalal and A. Hellal, *J. Ind. Eng. Chem.*, **20**, 2256 (2014).
- D. Shao, G. Sheng, C. Chen, X. Wang and M. Nagatsu, *Chemosphere*, **79**, 679 (2010).
- M.A. Shaker and A.A. Yakout, *Spectrochim. Acta A*, **154**, 145 (2016).
- L.A. Al-Khateeb, A.Y. Obaid, N.A. Asiri and M. Abdel Salam, *Ind. Eng. Chem.*, **20**, 916 (2014).
- K. Li, Y. Li and Z. Zheng, *J. Hazard. Mater.*, **178**, 553 (2010).
- F. Bhunia, N.C. Saha and A. Kaviraj, *Ecotoxicology*, **12**, 397 (2003).
- K.T. Chung, S.C. Chen, Y.Y. Zhu, T.Y. Wong and S.E. Stevens Jr., *Environ. Toxicol. Chem.*, **16**, 1366 (1997).
- D.H. Blakey, K.L. Maus, R. Bell, J. Bayley, G.R. Douglas and E.R. Nestmann, *Mutat. Res.*, **320**, 273 (1994).
- N.I. Sax, *Dangerous Properties of Industrial Materials*, Van Nostrand Reinhold Company Inc., New York (1984).
- D.S. Lee, K.S. Park, Y.W. Nam, Y.-C. Kim and C.H. Lee, *J. Hazard. Mater.*, **56**, 247 (1997).
- J.H. Sun, S.P. Sun, M.H. Fan, H.-Q. Guo, L.-P. Qiao and R.-X. Sun, *J. Hazard. Mater.*, **148**, 172 (2007).
- S. Gautam, S.P. Kamble, S.B. Sawant and V.G. Pangarkar, *Chem. Eng. J.*, **110**, 129 (2005).
- A. Saupe, *Chemosphere*, **39**, 2325 (1999).
- K. Zheng, B.C. Pan, Q.J. Zhang, W. Zhang, B. Pan, Y. Han, Q. Zhang, D. Wei, Z. Xu and Q. Zhang, *Sep. Purif. Technol.*, **57**, 250 (2007).
- Y.Q. Wu, M. Zhou, M.-G. Ma, Y. Zhang and H. Chen, *Technol. Water Treat. (China)*, **33**, 14 (2007).
- M.A. Oturan, J. Peiroten, P. Chartrin and A.J. Acher, *Environ. Sci. Technol.*, **34**, 3474 (2000).
- M. Suzuki, *Carbon*, **32**, 577 (1994).
- C. Brasquet and P. Le Cloriec, *Carbon*, **35**, 1307 (1997).
- I. Martín-Gullón and R. Font, *Water Res.*, **35**, 516 (2001).
- P.A. Quinlivan, L. Li and D.R.U. Knappe, *Water Res.*, **39**, 1663 (2005).
- K. Li, Z. Zheng, J. Feng, J. Zhang, X. Luo, G. Zhao and X. Huang, *J. Hazard. Mater.*, **166**, 1180 (2009).
- H. Shi, D. Shi, C. Li, S. Luan, J. Yin and R.K.Y. Li, *Mater. Lett.*, **133**, 200 (2014).
- A.S. Tsiamaki, S.K. Georgantzinou and N.K. Anifantis, *Sens. Actuators A*, **217**, 29 (2014).
- R.K. Joshi, P. Carbone, F.C. Wang, V.G. Kravets, Y. Su, I.V. Grigorieva, H.A. Wu, A.K. Geim and R.R. Nair, *Science*, **343**, 752 (2014).
- K. Yang, L. Feng, X. Shi and Z. Liu, *Chem. Soc. Rev.*, **42**, 530 (2013).
- A.K. Geim and K.S. Novoselov, *Nat. Mater.*, **6**, 183 (2007).
- L.A. Al-Khateeb, S. Almotiry and M.A. Salam, *Chem. Eng. J.*, **248**, 191 (2014).
- A.A. Yakout and M.A. Shaker, *J. Taiwan Inst. Chem. Eng.*, **63**, 81 (2016).
- T. Jiang, W. Liu, Y. Mao, L. Zhang, J. Cheng, M. Gong, H. Zhao, L. Dai, S. Zhang and Q. Zhao, *Chem. Eng. J.*, **259**, 603 (2015).
- X.L. Zhao, Y.L. Shi, Y.Q. Cai and S.F. Mou, *Environ. Sci. Technol.*, **42**, 1201 (2008).
- J.D. Li, X.L. Zhao, Y.L. Shi, Y.Q. Cai, S. Mou and G. Jiang, *J. Chromatogr. A*, **1180**, 24 (2008).

36. W. Yantasee, C.L. Warner, T. Sangvanich, R.S. Addleman, T.G. Carter, R.J. Wiacek, G.E. Fryxell, C. Timchalk and M.G. Warner, *Environ. Sci. Technol.*, **41**, 5114 (2007).
37. L. Cumbal and A. Sengupta, *Environ. Sci. Technol.*, **39**, 6508 (2005).
38. A.A. Yakout and H.M. Albishri, *J. Taiwan Instit. Chem. Eng.*, **55**, 180 (2015).
39. W.S. Hummers Jr. and R.E. Offeman, *J. Am. Chem. Soc.*, **80**, 1339 (1958).
40. N.I. Kovtyukhova, P.J. Ollivier, B.R. Martin, T.E. Mallouk, S.A. Chizhik, E.V. Buzaneva and A.D. Gorchinskiy, *Chem. Mater.*, **11**, 771 (1999).
41. V. Chandra, J. Park, Y. Chun, J.W. Lee, I.C. Hwang and K.S. Kim, *ACS Nano*, **4**, 3979 (2010).
42. Y. Guo, L. Deng, J. Li, S. Guo, E. Wang and S. Dong, *ACS Nano*, **5**, 1282 (2011).
43. S. He, B. Song, D. Li, C. Zhu, W. Qi, Y. Wen, L. Wang, S. Song, H. Fang and C. Fan, *Adv. Funct. Mater.*, **20**, 453 (2010).
44. J. Geng and H.-T. Jung, *J. Phys. Chem. C*, **114**, 8227 (2010).
45. Y. Xu, Z. Liu, X. Zhang, Y. Wang, J. Tian, Y. Huang, Y. Ma, X. Zhang and Y. Chen, *Adv. Mater.*, **21**, 1275 (2009).
46. J.C. Ma and D.A. Dougherty, *Chem. Rev.*, **97**, 1303 (1997).
47. H. Freundlich, *Z. Phys. Chem.*, **57**, 385 (1906).
48. I. Langmuir, *J. Am. Chem. Soc.*, **38**, 2221 (1916).
49. T.W. Weber and R.K. Chakravorti, *J. Am. Inst. Chem. Eng.*, **20**, 228 (1974).
50. D.O. Hayward and B.M.W. Trapnell, *Chemisorption*, Butterworths, London, edn 2 (1964).
51. S.J. Thomson and G. Webb, *Heterogeneous Catalysis*, Edinburgh, London, Oliver & Boyd (1968).
52. Y.S. Ho, *Scientometrics*, **59**, 171 (2004).
53. Y.S. Ho and G. McKay, *Process Biochem.*, **34**, 451 (1999).
54. S.H. Chien and W.R. Clayton, *Soil Sci. Soc. Am. J.*, **44**, 265 (1980).
55. S.K. Srivastava, R. Tyagi and N. Pant, *Water Res.*, **23**, 1161 (1989).
56. W. Liu, J. Zhang, C. Cheng, G. Tian and C. Zhang, *Chem. Eng. J.*, **175**, 24 (2011).